Molecular Systems Biology 8; Article number 604; doi:10.1038/msb.2012.35
Citation: ***Molecular Systems Biology*** **8:604**

www.molecularsystemsbiology.com

molecular systems biology

Dissecting sources of quantitative gene expression pattern divergence between *Drosophila* species

Zeba Wunderlich, Meghan D Bragdon, Kelly B Eckenrode, Tara Lydiard-Martin, Sivanne Pearl-Waserman and Angela H DePace*

Department of Systems Biology, Harvard Medical School, Boston, MA, USA
* Corresponding author. Department of Systems Biology, Harvard Medical School, 200 Longwood Avenue, Warren Alpert 536, Boston, MA 02115, USA.
Tel.: +1 617 432 7410; Fax: +1 617 432 5012; E-mail: angela_depace@hms.harvard.edu

Received 27.2.12; accepted 12.7.12

Gene expression patterns can diverge between species due to changes in a gene's regulatory DNA or changes in the proteins, e.g., transcription factors (TFs), that regulate the gene. We developed a modeling framework to uncover the sources of expression differences in blastoderm embryos of three *Drosophila* species, focusing on the regulatory circuit controlling expression of the *hunchback* (*hb*) posterior stripe. Using this framework and cellular-resolution expression measurements of *hb* and its regulating TFs, we found that changes in the expression patterns of *hb*'s TFs account for much of the expression divergence. We confirmed our predictions using transgenic *D. melanogaster* lines, which demonstrate that this set of orthologous *cis*-regulatory elements (CREs) direct similar, but not identical, expression patterns. We related expression pattern differences to sequence changes in the CRE using a calculation of the CRE's TF binding site content. By applying this calculation in both the transgenic and endogenous contexts, we found that changes in binding site content affect sensitivity to regulating TFs and that compensatory evolution may occur in circuit components other than the CRE.
Molecular Systems Biology **8**: 604; published online 14 August 2012; doi:10.1038/msb.2012.35
Subject Categories: metabolic and regulatory networks; development; chromatin & transcription
Keywords: cis-regulatory elements; gene expression divergence; transcriptional regulatory network

Introduction

Changes in gene expression patterns drive phenotypic change between both individuals and species (Gompel *et al*, 2005; McGregor *et al*, 2007; Wittkopp *et al*, 2008; Chan *et al*, 2010; Frankel *et al*, 2011). Many studies have identified dramatic gene expression changes, such as the gain or loss of an expression pattern, that underlie morphological phenotypes. Though more difficult to detect, small quantitative changes in gene expression may also lead to phenotypic variation between individuals and the evolution of new phenotypes between species (Brem *et al*, 2002; Wittkopp *et al*, 2009; Rockman *et al*, 2010). Indeed, quantitative variation in gene expression is pervasive within and between species, for example (Hutter *et al*, 2008; Nuzhdin *et al*, 2008; Cheung and Spielman, 2009; Muller *et al*, 2012). A fundamental challenge is to contextualize quantitative expression variation: what are its sources and its phenotypic consequences?

Gene expression occurs in the context of a network. The expression pattern of any given gene is dependent on the expression of its regulators. Information about the position and level of regulators is integrated by regulatory DNA, e.g., promoters, *cis*-regulatory elements (CREs or enhancers), and 3′ and 5′ untranslated regions (UTRs). Any part of a regulatory network can change between species, obscuring the underlying mechanism of expression pattern conservation and divergence. For example, if the expression pattern of a gene has changed, then this could be due to changes in the expression of upstream regulators or changes in any of the relevant pieces of regulatory DNA. Reciprocally, if an expression pattern is conserved, then either the expression patterns of upstream regulators and the function of regulatory DNA are conserved or changes in one component have been compensated for by changes in another.

To contextualize gene expression changes between species, it is therefore ideal to examine the expression patterns of the entire network simultaneously. Practically, there is a trade-off between measuring all network components comprehensively and measuring them in multiple cell types. Single-celled organisms are amenable to comprehensive measurements of gene expression using genome-wide techniques, i.e., RNA-seq. These types of studies have revealed widespread rewiring of transcriptional networks, even in cases where the output of the circuits is conserved, reviewed in Li and Johnson (2010). Making comprehensive measurements in animals is more technically challenging since an organism is composed of multiple cell types with distinct gene expression profiles. Genome-scale techniques are not spatially resolved, as they require whole organisms or tissues to be homogenized. Imaging techniques offer spatial resolution and are increasingly quantitative but are often limited to only a few genes. For example, in insects, comparative studies of small numbers of genes have shown both cases where gene expression patterns appear conserved in the face of changing regulatory sequence

(Lukowitz *et al*, 1994; Ludwig *et al*, 2000; Wittkopp *et al*, 2003; Wratten *et al*, 2006; Hare *et al*, 2008a; Swanson *et al*, 2011) and cases where expression patterns diverge (Ludwig *et al*, 2005; Zinzen *et al*, 2006; Goltsev *et al*, 2007; Lott *et al*, 2007; Crocker *et al*, 2008; Fowlkes *et al*, 2011). Here, we pursue a strategy that is intermediate between these two extremes—simultaneous measurement of a small number of relevant network components, in multiple species, at cellular resolution.

As a model system to develop this approach, we use the conserved developmental transcriptional network that patterns the anterior-posterior axis in *Drosophila* embryos. This network exhibits quantitative differences in spatial and temporal expression patterns across multiple closely related species (Fowlkes *et al*, 2011). We recently completed a survey of gene expression in blastoderm embryos of *D. yakuba* (*dyak*) and *D. pseudoobscura* (*dpse*) (Fowlkes *et al*, 2011), which complements the existing data set for *D. melanogaster* (*dmel*) (Fowlkes *et al*, 2008). Our high-resolution imaging methods produce a gene expression atlas in which the relative expression levels for an arbitrary number of genes are mapped onto each cell in an average 3D embryo. These data are uniquely suited for identifying quantitative expression differences, as subtle differences in expression can be accurately measured. Our global analysis of these three data sets showed that individual genes differ quantitatively in their spatiotemporal gene expression patterns. However, cellular gene expression profiles, consisting of 13 genes in the anterior-posterior patterning network, are mostly conserved, implying that regulatory relationships between these genes are also largely conserved.

Here, we develop and apply a computational framework to assess the sources of expression divergence for an individual regulatory circuit in this network. We define a regulatory circuit to be the inputs and output of an individual CRE (Ben-Tabou de-Leon and Davidson, 2007). A gene can be controlled by multiple CREs, each of which controls a portion of the gene expression pattern in space and time. In this study, we define the inputs to be the regulating transcription factors (TFs) of a CRE and the output to be the portion of the expression pattern directed by the CRE. However, our general strategy can also be extended to accommodate other components of transcriptional regulatory circuits. This approach allows us to: (1) quantify the behavior of the circuit across species; (2) attribute the sources of expression divergence either to changes in the expression patterns of upstream regulators or to changes in the regulatory logic of the circuit; and (3) assess the contributions of changes in CRE sequence to the expression output.

As a case study, we examine the circuit that controls the hunchback (*hb*) posterior stripe. *hb* is a widely conserved zinc-finger TF near the top of the anterior-posterior segmentation network hierarchy (Lehmann and Nüsslein-Volhard, 1987; Struhl *et al*, 1992; Lukowitz *et al*, 1994; Lynch and Desplan, 2003). *hb* is expressed in two regions at the blastoderm stage: a broad anterior domain, which is largely maternally controlled, and a posterior stripe, which is solely due to zygotic transcription (Figure 1A; Lehmann and Nüsslein-Volhard, 1987; Tautz *et al*, 1987; Schröder *et al*, 1988). The *hb* posterior stripe expression pattern varies quantitatively between *dmel*, *dyak*, and *dpse* (Fowlkes *et al*, 2011). From extensive experimental data, we know *hb*'s input TFs and the structure of the CREs in its locus (Jäckle *et al*, 1986; Casanova, 1990; Margolis *et al*, 1995; Kosman and Small, 1997). Like many other CREs in the network, the TF binding site content of the *hb* posterior stripe CRE varies significantly across these three Drosophilids (Moses *et al*, 2006; Kim *et al*, 2009), whose last common ancestor lived ~25 million years ago (Figure 1B; Richards *et al*, 2005).

Our approach is to first define an input/output function that relates the concentration of regulating TFs to the observed expression pattern in individual cells. We then assess the degree of conservation of the circuit's input/output function by fitting the function in each of the three *Drosophila* species. Because these functions operate at cellular resolution, we can quantify the extent to which expression divergence is due to upstream changes in the expression patterns of regulating TFs. We validate our predictions using CRE reporter constructs in transgenic animals in which all inputs are constant and only the sequence of the CRE is changing. We also use these transgenic data to calculate the CRE sequence contribution to the input/output function without fitting additional parameters; this calculation is based on predicted TF binding sites in the set of orthologous CREs. Finally, we add this calculation of CRE sequence contribution to the input/output function in the endogenous context to assess the contribution of CRE sequence to the behavior of the native regulatory circuit.

Using this strategy, we found that there is a large degree of functional conservation in the *hb* posterior stripe circuit. The majority of the endogenous gene expression divergence is due to positional shifts in expression of *hb*'s regulators. We found that the calculated CRE sequence contribution improves the fit of the input/output function in the transgenic context. We conclude that small changes in CRE sequence do have functional consequences; they alter sensitivity to regulating TFs. This has implications for current models of CRE function, where the degree of flexibility in the arrangement of TF binding sites is a matter of debate (Crocker and Erives, 2008; Hare *et al*, 2008a, b). We found that adding the CRE sequence contribution to the input/output function in the endogenous context leads to mixed results, implying that orthologous TFs in these species may not be functionally identical, as is widely assumed, or that compensatory evolution has occurred outside of the CRE. We discuss the implications of these results for understanding transcriptional circuit evolution with quantitative precision.

Results

There are quantitative differences in the *hb* expression pattern between species

The endogenous expression pattern of *hb* was previously measured at cellular resolution in *dmel*, *dyak*, and *dpse* (Fowlkes *et al*, 2008, 2011; Figure 2A). Briefly, expression was visualized using RNA fluorescent *in-situ* hybridization against *hb* and a fiduciary marker (see Materials and methods). The *in-situ* protocol uses an amplification step to improve the signal to noise ratio. We find no evidence that this protocol results in non-linear amplification of signal (Supplementary Figure 1). The stained embryos were imaged using 2-photon laser scanning microscopy, and automated image analysis

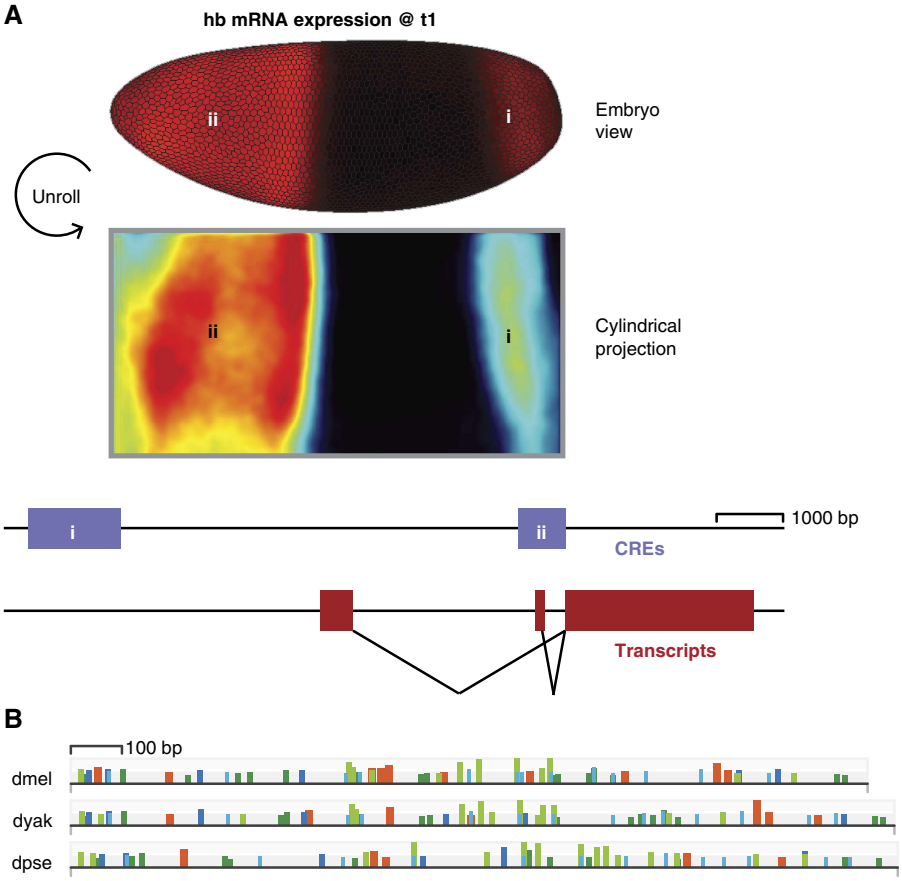

Figure 1 The two spatial domains of the *hb* expression pattern are driven by two CREs. (**A**) *hb* is expressed in a broad anterior domain and a posterior stripe in blastoderm-age embryos. We show two views of the *dmel hb* mRNA expression pattern at the first time point from the *dmel* atlas (Fowlkes *et al*, 2008). On top is a rendering in a typical dorsolateral embryo view, where expression is in red with brightness proportional to level. On bottom is a cylindrical projection, where high expression is in red and low expression is in blue. In both views, anterior is to the left and dorsal is up. Below the expression patterns, we show the structure of the *hb* locus, with regulatory elements in purple and transcripts in red. The expression pattern is controlled by two CREs, one driving the anterior domain (ii) and one driving the posterior stripe (i). The two *hb* transcript isoforms are functionally identical, and both transcripts contribute to both spatial expression domains (Margolis *et al*, 1995). (**B**) The binding site content of the *hb* posterior stripe CRE varies between species. We plot the predicted TF binding sites of *hb*'s regulators in the sequences of orthologous *hb* posterior stripe CREs from *D. melanogaster* (*dmel*), *D. yakuba* (*dyak*), and *D. pseudoobscura* (*dpse*) (see Materials and methods). *hkb* sites are highlighted in orange and *tll*, *kni*, *Kr*, and *gt* sites are shown as light blue, dark blue, light green, and dark green rectangles, respectively. The height of the rectangle is proportional to binding site strength and the width of the rectangle is proportional to the length of the binding site.

techniques were used to convert image data into PointClouds, text files that contain the spatial coordinates and expression levels of *hb* and the fiduciary marker in each nucleus (Luengo Hendriks *et al*, 2006). Each of the PointClouds was then matched to a species-specific embryo template using the fiduciary marker (Fowlkes *et al*, 2008). Once all the embryos are mapped onto the template, average *hb* expression values are calculated for each cell at each time point. Since expression can only be measured in relative units with this *in-situ* protocol, each gene's expression values are normalized so that the minimum value is 0 and the 95th percentile value corresponds to 1. The resulting gene expression atlases contain the average values of *hb* expression derived from 5 to 29 embryos for each of six time intervals during the hour of blastoderm-stage development. The resulting gene expression patterns are qualitatively similar: each species has a *hb* posterior stripe, but they vary quantitatively in relative position, particularly in the earlier time points, and in the width of the stripe (Figure 2B and C).

A modeling framework to understand the origins of *hb* gene expression divergence between species

Many factors may cause the observed inter-species divergence in the *hb* expression pattern. Changes in any part of a gene's regulatory DNA or the expression patterns of the regulatory molecules that bind this DNA can influence a gene's expression pattern (Maston *et al*, 2006; Consortium *et al*, 2010). Given our cellular resolution data set, we are best equipped to assess the influence of spatially varying inputs on a gene's output. We therefore restrict our considerations to *hb*'s input TFs and the CRE that integrates these inputs. We then separate potentially influential changes in the circuit into two categories: differences in the expression patterns of *hb*'s input TFs, which we call *positional information*, and differences in *hb*'s sensitivity to its inputs, which we call *regulatory logic*. The terms *trans* and *cis* are often used to denote these contributions to expression divergence, but we decided against these terms for two reasons. First, in studies

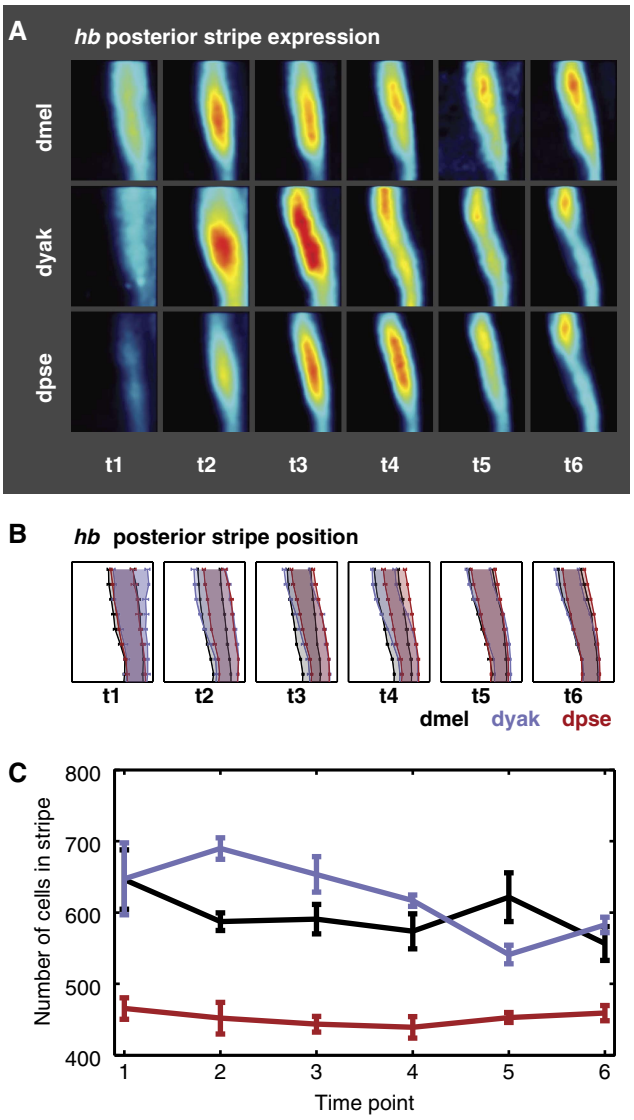

Figure 2 *hb* patterns differ between three *Drosophila* species. (**A**) The *hb* posterior stripe expression pattern diverges between three species. We show the average expression patterns in the posterior 36% of embryos for the endogenous *hb* pattern in *dmel*, *dyak*, and *dpse*, at six time points spanning the hour of blastoderm-stage development. The panels are oriented with the anterior end to the left and the dorsal side on the top, and the levels are indicated by the color, where black is no expression and red is high expression. The shape and dynamics of the *hb* posterior stripe expression pattern vary between the three species. (**B**) The average *hb* posterior stripe boundary locations vary between species at early time points. We plot the average boundary locations of the *hb* posterior stripe in percentage egg length. The panels are oriented in the same manner as (A). Average boundary positions are shown for *dmel* in black, *dyak* in purple, and *dpse* in red, for six time points. Error bars denote the standard error of the mean. (**C**) The average number of cells in the *hb* posterior stripe varies between species at all time points. We plot the average number of cells in the *hb* posterior stripe for *dmel*, *dyak*, and *dpse* for six time points. Error bars denote the standard error of the mean. *dpse* embryos have fewer total cells than *dmel* and *dyak* embryos. Therefore, the number of cells in the *dpse hb* posterior stripe is much smaller than in *dyak* and *dmel* stripes, even though its size as a fraction of egg length is similar. Source data is available for this figure in the Supplementary information.

that concern gene expression divergence, *trans* is often used to connote changes in TF coding sequences. Here, *positional information* only refers to changes in the expression pattern of the TFs. Second, our use of *positional information* is consistent with the definition traditionally used in developmental biology, i.e., the spatially varying expression patterns of molecules that determine cell type.

Our modeling framework is designed to disentangle the contributions of changes in positional information and regulatory logic to *hb* expression divergence by modeling gene expression in single cells. We first define a function that relates inputs to outputs in individual cells, Equation (1). If the change in the output expression pattern between species is due to a change in the position of an upstream regulator, i.e., a change in positional information, then we expect this function to accurately predict expression of the output based on the concentration of inputs across all cells in each species. However, the cells will occur in different locations because the spatial pattern of the inputs differs.

$$hb(i, s) = f(\mathbf{r}(i, s), \mathbf{k}) \quad (1)$$

Here, $hb(i, s)$ is the measured *hb* gene expression level in cell i in species s, $\mathbf{r}(i, s)$ is a vector containing the corresponding expression levels of *hb*'s regulators, $\mathbf{k}$ is a vector consisting of coefficients describing the effect of each TF on *hb*, i.e., the strength of repression or activation per expression unit of the TF, and f is a function relating $\mathbf{r}$ and $\mathbf{k}$ to *hb*.

In contrast, if the expression difference is due to a change in regulatory logic, i.e., the circuit is responding to an upstream input differently, then we would expect a difference in the relationship of input and output concentrations. We can incorporate this into Equation (1) by including a species-specific vector $\mathbf{k}(s)$ to relate the levels of regulators to the level of *hb*. Equation (2) therefore describes the scenario in which the divergence in the *hb* pattern is caused by both changes in positional information and regulatory logic.

$$hb(i, s) = f(\mathbf{r}(i, s), \mathbf{k}(s)) \quad (2)$$

Given a functional form, we call the fit of Equation (2) to each species' own data the *best fit*; it is the best performance possible given that functional form. To determine whether a regulatory circuit is conserved, we can fit the function in one species using Equation (1), use those fit parameters to predict expression in the other species (we call this the *applied fit*), and compare the performance of the model to the *best fit*. If the contribution of positional information is large relative to changes in regulatory logic, then these two fits will be similar. If the contribution of positional information is small, then the *best fit* will be much better than the *applied fit*.

To implement this framework for the *hb* posterior stripe, we must make several choices regarding the inputs of the circuit, the use of the six time points in our data set, and the form of the function f. We chose the five primary regulators of *hb*'s posterior stripe defined by genetic analyses: *giant*, *gt*; *huckebein*, *hkb*; *knirps*, *kni*; *Krüppel*, *Kr*; and *tailless*, *tll* (Jäckle *et al*, 1986; Casanova, 1990; Margolis *et al*, 1995; Kosman and Small, 1997). These genes are all in gene expression atlases for *dmel*, *dyak*, and *dpse* (Fowlkes *et al*, 2008, 2011). We excluded *caudal*, a potential activator of *hb*, because *caudal* is not in the *dpse* atlas due to low level staining (Fowlkes *et al*, 2011). Thus, *caudal*'s contribution is not spatially localized in our model and is instead included in the constant term in Equation (3) (see Discussion). The time

points in the atlases correspond to ~10 min intervals. Because transcription can occur on the timescale of a few minutes (Ardehali and Lis, 2009), we assume that target expression levels can be predicted from regulators' expression levels at the same time point and therefore use all time points to fit our function simultaneously. Adding a time delay of one 10 min time step between the inputs and outputs improved the modeling accuracy but reduced the total size of our data set. Because excluding a single time point can create a similar increase in modeling accuracy, we did not use a time delay in subsequent analyses (Supplementary Figure 2). There are many functional forms we could use for f. We first consider a simple linear form. Explicitly, Equations (1) and (2) correspond to

$$\begin{aligned} hb(i,\,s,\,t) &= \mathbf{r}(i,\,s,\,t)\,\cdot\,\mathbf{k} + a \\ &= k^{gt}\,\cdot\,gt(i,\,s,\,t) + k^{hkb}\,\cdot\,hkb(i,\,s,\,t) \\ &\quad + k^{kni}\,\cdot\,kni(i,\,s,\,t) + k^{Kr}\,\cdot\,Kr(i,\,s,\,t) \\ &\quad + k^{tll}\,\cdot\,tll(i,\,s,\,t) + a \end{aligned} \tag{3}$$

$$\begin{aligned} hb(i,\,s,\,t) &= \mathbf{r}(i,\,s,\,t)\,\cdot\,\mathbf{k}(s) + a(s) \\ &= k_s^{gt}\cdot gt(i,\,s,\,t) + k_s^{hkb}\cdot hkb(i,\,s,\,t) + k_s^{kni}\cdot kni(i,\,s,\,t) \\ &\quad + k_s^{Kr}\,\cdot\,Kr(i,\,s,\,t) + k_s^{tll}\,\cdot\,tll(i,\,s,\,t) + a(s) \end{aligned} \tag{4}$$

The constants a and $a(s)$ and the coefficients $\mathbf{k}$ and $\mathbf{k}(s)$ were fit using standard methods for multiple linear regression.

To evaluate the model fits, we compared the predicted levels of *hb* expression with the measured values using the area under a receiver operating characteristic curve (ROC AUC) (Swets, 1988). ROC curves compare the predictions from the model with the experimental data in a binary manner; this requires us to threshold both the experimental data and the predictions to score them relative to one another. Importantly, we did not threshold the data for the purpose of prediction, only for the purposes of scoring. For each cell, we determined whether *hb* is 'on' or 'off' in the experimental data using a different threshold for each species or transgenic line (Materials and methods). For the modeling results, we varied the threshold separating 'on' from 'off' cells. For each threshold, we calculated true positive and false positive rates, plotted these rates against each other to create the ROC curve, and calculated the area underneath it (Supplementary Figure 3). An AUC of 1 corresponds to a perfect classifier, and an AUC of 0.5 corresponds to a random classifier. We used this measure because it is not influenced by the experimental noise in 'off' cells and potential global changes in levels between species. Furthermore, though we find no evidence for non-linearities in our measurements (Supplementary Figure 1), the ROC AUC is not very sensitive to potential non-linearities (Supplementary information). An alternate measure of model performance (the r^2 value) also supports our conclusions (Supplementary Figure 4).

The majority of *hb* expression pattern divergence is due to changes in positional information

To test the capability of a linear model to recapitulate each species' *hb* pattern, we fit the $\mathbf{k}(s)$ vector in Equation (4) using the posterior 36% of the each species' embryo, which corresponds to the location of the endogenous *dmel hb* posterior stripe ±10% of the egg length. The linear model fits the endogenous *hb* expression in each species with AUC = 0.95, 0.96, and 0.95 for *dmel*, *dyak*, and *dpse*, respectively (Figure 3A; P-values < 0.001 using the Mann–Whitney U-test). The coefficients resulting from this fit are shown in Table I.

To assess the contribution of changing positional information to expression pattern divergence, we compared the performance of the linear model using a single set of $\mathbf{k}$ values, the applied fit, to the performance using species-specific $\mathbf{k}(s)$, the best fit. Specifically, we fit the model in *dmel*, and applied the fit parameters to the other species. We found that using the *dmel* parameters, $\mathbf{k}(dmel)$, recapitulates most of the performance in *dyak* and *dpse* (AUC = 0.93 and 0.94, respectively; Figure 3A; P-values < 0.001 using the Mann–Whitney U-test). We also conducted an error propagation analysis to ensure that differences in the applied fits are not due to differences in measurement error between species. We find that a conservative estimate of the effect of measurement error on the AUC is smaller than the differences we interpret as significant (Supplementary information).

These results indicate that a large fraction of *hb* expression divergence is explained by changes in the positional information of *hb*'s upstream regulators. A detailed view of the model performance (Figure 3B) shows that changes in positional information cause notable differences between species, e.g., the narrow stripe at the first time point of *dpse* and the wide stripe at the second two time points of *dyak* (see columns 1–3 of Figure 3B). This result implies that the regulatory logic between *hb* and its regulators is largely conserved between *dmel*, *dyak*, and *dpse*.

Though the applied fit is an excellent predictor of *hb* expression, a statistical comparison shows that there is a significant difference between the best fits and applied fits for both *dyak* and *dpse* (P-values < 0.001 using the Mann–Whitney U-test), indicating there is not complete conservation of the regulatory logic. We explore the contributions of sequence divergence in the orthologous CREs to these differences in later sections.

We performed several additional calculations to test the assumptions of our model. When we fit the linear model to the entire embryo at once, the performance of the model drops substantially (Supplementary Figure 5), implying that there is more than one input/output function creating the endogenous *hb* pattern. We expect this because there are multiple CREs in the locus. The model performance did not improve substantially upon the addition of higher order terms and is worse when any regulator is excluded (Supplementary Figure 6). Ten-fold cross-validation confirms that the model is not over-fit to the data (Supplementary Figure 7).

Transgenic experiments show the changes in regulatory logic encoded by orthologous *hb* posterior stripe CREs

Our model indicates that the regulatory logic of this circuit is largely conserved but exhibits quantitative differences between species. These differences could be due to changes in activity or level of input TFs or changes in the CRE,

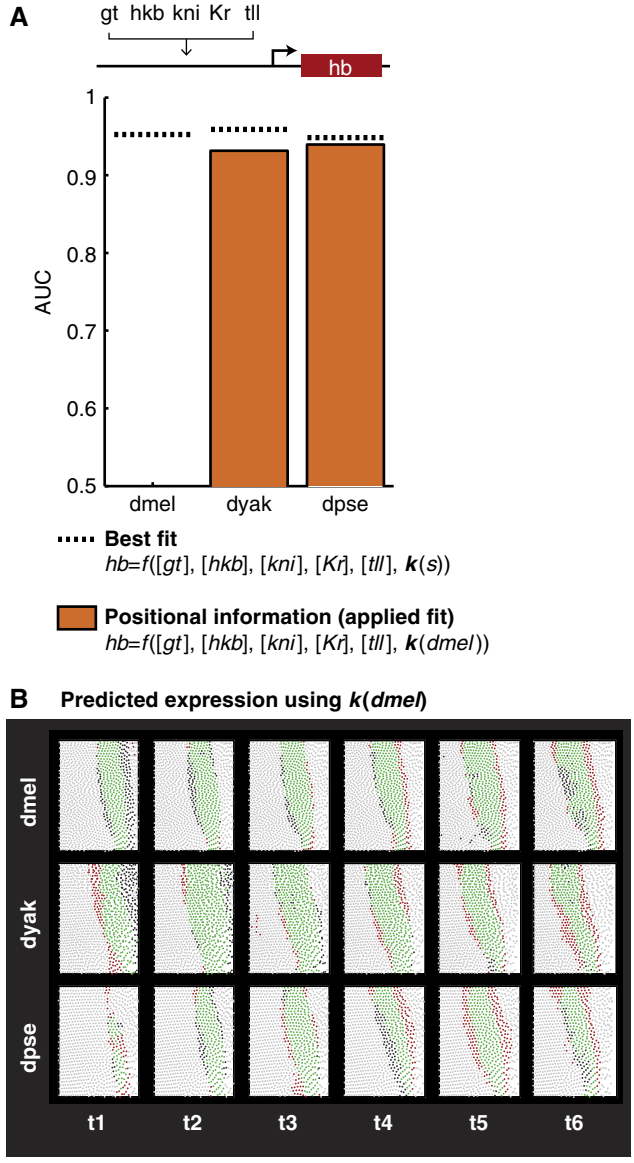

Figure 3 A linear model fits endogenous *hb* expression patterns with high accuracy. (**A**) Changes in positional information account for a large portion of *hb* expression pattern divergence. Here, we show the results of fitting a multiple linear regression model to the endogenous *hb* pattern in each species (dotted line, best fit) and by fitting to *dmel* and applying the resulting coefficients to the *hb* patterns in *dyak* and *dpse* (orange bars, positional information). Performance of the model was measured using the area under the ROC curve (AUC), and the results are plotted for the species in order or increasing phylogenetic distance from *dmel*. (**B**) Differences in the *hb* expression pattern can be explained using a common parameter set. We show the detailed results of the positional information model, using *k*(*dmel*). For the sake of visualization, we found a threshold for each species that yielded an 80% true positive rate. This corresponds to a single point on the ROC curve that we integrated to calculate the AUC scores shown in (A). Each circle in the subpanels corresponds to a cell, with green and light gray circles corresponding to correct predictions in which the cell is on (green) or off (light gray) in the experimental data. The red and dark gray cells correspond to incorrect predictions, in which the cell is off (red) or on (dark gray) in the experimental data.

promoter, or UTRs. Indeed, all of these sequence components differ between species. We tested whether sequence variation in the *hb* posterior stripe CRE leads to quantitative expression differences for two reasons. First, CREs dictate the wiring of the circuit; they integrate information about the input TF concentrations to produce a particular output. Second, they are a well-characterized regulatory component of the circuit, making comparative bioinformatics analysis tractable.

Table I Coefficient values resulting from the multiple linear regression to the endogenous data sets (best fit)

s	dmel	dyak	dpse
$a(s)$	0.483	0.569	0.429
k_s^{hkb}	−0.497	−0.293	−0.306
k_s^{gt}	−0.566	−1.05	−0.730
k_s^{kni}	−0.418	−0.913	−0.435
k_s^{Kr}	−0.429	−0.628	−0.0914
k_s^{tll}	0.170	0.0707	0.0272

We tested whether this set of orthologous CREs direct quantitatively different expression patterns by making transgenic reporters in *dmel*, where all inputs are identical and only the CRE sequences differ. These reporters drive the expression of *lacZ*. All constructs were integrated into the *dmel* genome at the same site (Materials and methods). We created transgenic lines for the *dmel*, *dyak*, *dpse*, and *D. persimilis* (*dper*) *hb* CREs. Because *dpse* and *dper* are closely related, we expect the expression driven by these two CREs to be more similar to each other than to *dmel* or *dyak*. This comparison gives an informal sense of the error in our experimental and analytical techniques. For each transgenic line, we measured *lacZ* expression levels in four or more embryos per time point (Materials and methods). We combined the data for the transgenic constructs with the existing *dmel* expression atlas (Fowlkes *et al*, 2008), resulting in a data set that includes cellular resolution measurements of both the inputs and output of each CRE. This data set allowed us to measure the input/output function of each CRE and detect quantitative differences in their regulatory logic.

The expression patterns driven by these orthologous CREs are similar but differ quantitatively in stripe location and width (Figure 4). The orthologous CREs also drive variable amounts of expression in the anterior (Supplementary Figure 8, see Discussion). Given the common positional information, observed differences must be entirely due to sequence changes between the CREs.

We tested the effects of these sequence changes on the regulatory logic of the circuit using our computational framework. To do this, we write Equation (1) as

$$lacZ(i, s, t) = \mathbf{r}(i, t) \cdot \mathbf{k} + a \qquad (5)$$

where $lacZ(i, s, t)$ is the expression value of *lacZ* driven by the CRE from species s in cell i at time t, $\mathbf{r}$ is a 1×5 vector of the expression values of *hb*'s five regulators in the corresponding cell, $\mathbf{k}$ is a 5×1 vector of coefficients describing the effect of each regulator on *lacZ*'s expression pattern, and a is a constant. We fit the $\mathbf{k}$ vector in Equation (5) to the *dmel* transgenic data set using the posterior 36% of the embryo.

The linear model fits the *dmel* data with AUC = 0.94 (Figure 5; P-value < 0.001 using the Mann–Whitney U-test). We applied the same coefficient vector $\mathbf{k}$ to the other transgenic data sets without re-fitting. The range of AUCs resulting from this analysis, 0.88–0.91 (P-values < 0.001 using the Mann–Whitney U-test), indicate that though largely

similar, there are quantitative differences between the regulatory logic encoded by the orthologous CREs. Cross-validation showed that the linear model is not over-fit to the data (Supplementary Figure 9).

A simple sequence-based calculation accounts for changes in the regulatory logic encoded by orthologous CREs

In the transgenic experiments, the only possible source of regulatory logic divergence is sequence divergence in the CREs. We therefore attempted to calculate the sequence contribution to $\boldsymbol{k}(s)$ using predicted TF binding sites in the CREs.

Theoretically, $\boldsymbol{k}$ reflects a combination of each regulator's intrinsic potency and its capacity to act on the CRE, e.g., the number and strength of its binding sites. Since all transgenics share the same *dmel* environment, the potency of the regulators is the same for all lines, and only their capacity to act changes. We express each element i of $\boldsymbol{k}(s)$ as

$$k_i(s) = p_i \cdot c_i(s) \tag{6}$$

where p_i is the potency of regulator i, and $c_i(s)$ is its capacity. We set all the values of $\boldsymbol{c}(dmel)$ to 1, so $\boldsymbol{k}(dmel) = \boldsymbol{p}$ and is unchanged from the calculation done for Equation (5). To calculate $\boldsymbol{c}(s)$, which we call a 'sequence weight,' for the other transgenic lines, we use a formula that corresponds to the total strength of each regulator's predicted binding sites in each CRE, normalized to the total strength in the *dmel* CRE (Materials and methods; Figure 5B). In principle, the sequence weight could be calculated in other ways; however, as we show below, this simple calculation is informative in our framework.

The addition of this sequence weight improves the fit of the input/output function to the data (Figure 5A and C; AUCs = 0.92–0.97; comparison P-values < 0.001 using the Mann–Whitney U-test). The most dramatic improvements of prediction performance are for those species that are the most diverged from *dmel*. Increasing the influence of *gt* and *kni* and decreasing the influence of *hkb* in *dpse* and *dper* allows the model to more accurately recapitulate the *lacZ* expression pattern, specifically the extension of the stripe further to the posterior of the embryo, where *hkb* is expressed. The increase in model performance indicates that these orthologous CREs differ in sensitivity to their inputs, and we conclude that sequence changes in these CREs have functional consequences.

Though simple, the sequence weight is a useful calculation for predicting the effects of sequence changes on expression output. This is notable because the improvement in fit does not require fitting any extra parameters and because the sequence weight does not include any information about the

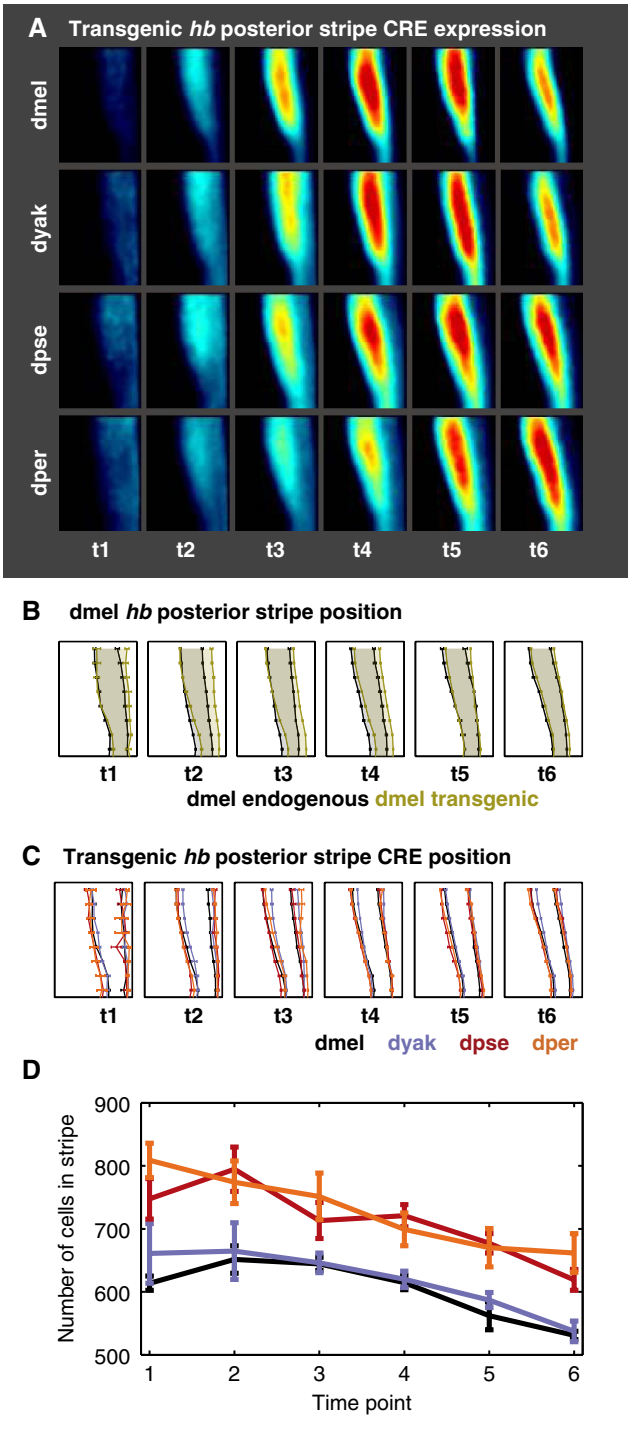

Figure 4 Orthologous CREs drive similar, but not identical expression patterns in transgenic *dmel* lines. (**A**) Expression patterns driven by orthologous *hb* posterior stripe CREs vary quantitatively. We show the average *lacZ* expression pattern in the posterior 36% of transgenic flies using the same conventions as Figure 2A. These patterns are measured in transgenic *dmel* lines containing the *hb* posterior stripe CRE from each of four species, driving a *lacZ* reporter. (**B**) The transgenic and endogenous *dmel hb* posterior stripe patterns are not identical. A comparison of the stripe boundary locations of the endogenous and transgenic *hb* posterior stripe indicate that the patterns are different, particularly at early time points. Here, we plot the average stripe boundary position for the *dmel* endogenous (black) and transgenic (olive) patterns, relative to total egg length, for six time points. The error bars show the standard error of the mean. (**C**) The transgenic *hb* posterior stripe boundary locations vary subtly between species. We plot the average boundary locations of the *hb* posterior stripe CRE in percentage egg length. Average boundary positions are shown for the *dmel* CRE in black, *dyak* in purple, and *dpse* in red, and *dper* in orange, for six time points. Error bars denote the standard error of the mean. (**D**) The average number of cells in the *hb* posterior stripe varies between some species at all time points. We plot the average number of cells in the *hb* posterior stripe CRE for *dmel*, *dyak*, *dpse*, and *dper* CREs for six time points. Error bars denote the standard error of the mean. This plot shows that a change in boundary position of ~1% egg length corresponds to a change of ~100 cells contained within the stripe. Source data is available for this figure in the Supplementary information.

arrangement of sites relative to one another. We presume this is not because local arrangement of sites is unimportant but rather because these orthologous CREs all contain functional arrangements of binding sites. If this is true, then an alternative method for calculating the sequence weight would be necessary to assess synthetic or non-orthologous CREs.

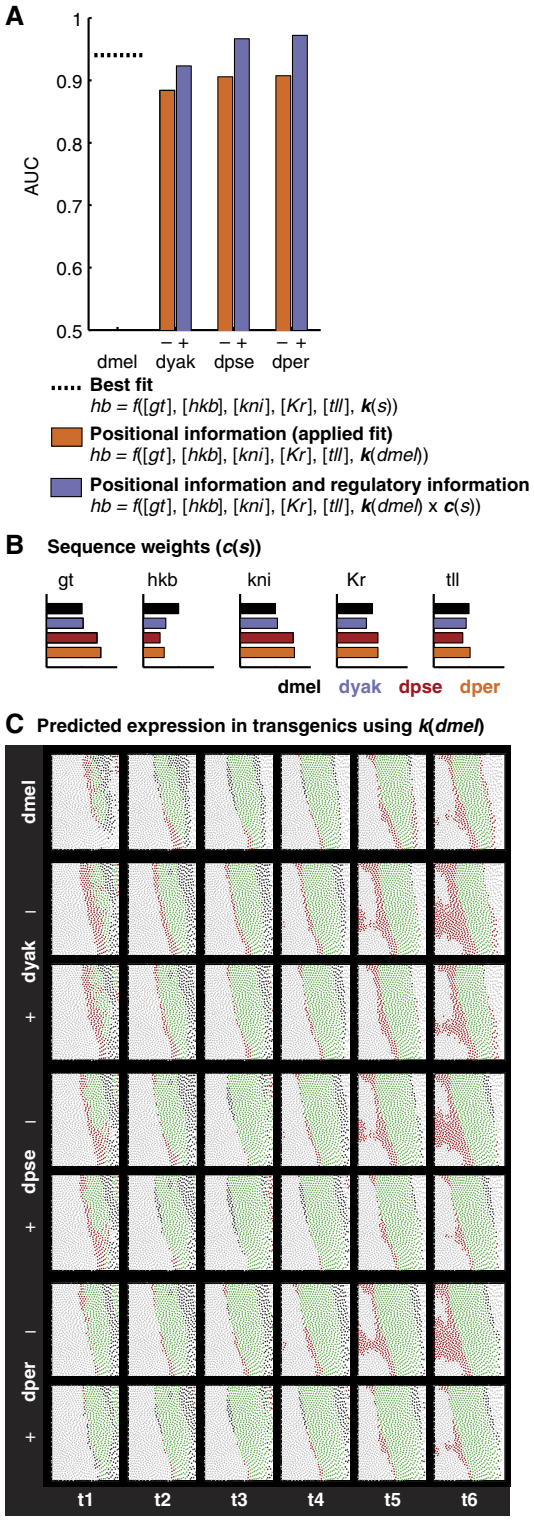

Sequence-based calculations of regulatory logic are only effective in the endogenous context at shorter phylogenetic distances

We applied the sequence weight calculation to the endogenous data sets. As explained above, $\boldsymbol{k}$ represents both the potency, $\boldsymbol{p}$, of each TF, and its capacity to act, $\boldsymbol{c}$, on the target. We assumed that $\boldsymbol{p}$ is conserved between species because of the high degree of coding sequence conservation of the TFs in this system. To predict binding sites in the other species, we also assumed that the DNA binding preferences determined for each *dmel* TF are valid for its orthologs in *dyak* and *dpse* (see Discussion). We then estimated the contribution of *cis*-regulatory changes by calculating $\boldsymbol{c}(s)$ as we did for the transgenic lines and multiplied these sequence weights to the corresponding values of $\boldsymbol{k}(dmel)$.

We found that the addition of the sequence weight to the predictions made using the $\boldsymbol{k}(dmel)$ parameter set improves the *dyak* predictions, increasing the AUC from 0.93 to 0.95, and worsens the *dpse* predictions, decreasing the AUC from 0.94 to 0.91 (Figure 6; comparison P-values <0.001, using the Mann–Whitney U-test). When compared with *dmel*, virtually all of the *hb* expression divergence in *dyak* is explained by changes in positional information and changes in regulatory logic due to sequence changes in the CRE. *dpse* is further diverged from *dmel* than *dyak*. Nearly all of *hb* expression divergence in *dpse* is explained by positional information. However, we cannot estimate all the changes in regulatory logic using only the sequence weight for the CRE. This is not because the sequence weight is ineffective for the *dpse hb* posterior stripe CRE (see transgenic results in Figure 5). Rather it may reflect the fact that many features of the locus, including other *hb* CREs, the promoter, and the UTRs, contribute to *hb* expression. These features are all presumably more diverged in *dpse* than in *dyak* as compared with *dmel*. Changes in these other components may overwhelm the effect of sequence changes in the *hb* posterior stripe CRE in the *dpse* endogenous context. Alternatively, *dpse* TFs may not be equivalent to their *dmel* counterparts in terms of their potency, DNA binding

Figure 5 The addition of sequence weights improves the fit of a linear model to the transgenic data. (**A**) Including CRE sequence information improves the fit of the linear model to the transgenic expression pattern. We show the results of fitting a multiple linear regression model to the transgenic line expressing *lacZ* under the control of the *dmel hb* posterior stripe CRE and applying the resulting coefficients to the other transgenic lines (orange bars, positional information). Adding a sequence weight, a scaling parameter that accounts for the differences in binding site content of the different posterior stripe CREs, improves the fit of the model to the data (purple bars, regulatory logic). (**B**) Sequence weights for the *hb* posterior stripe CRE. We plot the sequence weight for each TF and CRE, which roughly corresponds to the total binding potential for each TF along the CRE. The sequence weights are normalized so that they are 1 in *dmel* (black bars). (**C**) The addition of the sequence weight lowers the false positive predication rate. As in Figure 3, we visualize the results of the model at the 80% true positive rate. In each sub-panel, each circle corresponds to a cell, with the color indicating whether or not the model is correct. Green circles are cells that are correctly predicted to be on, light gray circles are cells that are correctly predicted to be off. Red circles are cells that are incorrectly predicted be to on, and dark gray circles are cells that are incorrectly predicted to be off. For each species, excluding *dmel*, we show the model performance without (− , top row) and with (+ , bottom row) the sequence weight.

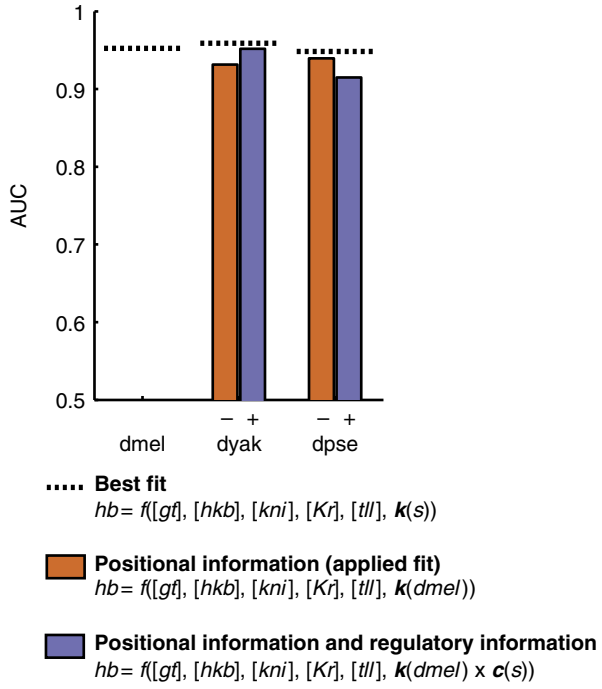

Figure 6 The addition of the sequence weight improves endogenous *dyak* predictions. We show the results of fitting a multiple linear regression model to the endogenous *hb* pattern using a species-specific parameter vector ***k***(*s*) (dotted line, best fit), the *dmel* parameter vector (orange bars, positional information), the *dmel* parameter vector and sequence weights (purple bars, regulatory information). The addition of a sequence weight improves the model fit in *dyak* and worsens the model fit in *dpse*.

preferences, or absolute gene expression levels, limiting our ability to fit the model or calculate the sequence weight.

Discussion

We present a method to investigate the origins of quantitative divergence in gene expression patterns. Because gene expression occurs in the context of a network, to compare any one component between species one must control for changes in other parts of the network. In the context of a single transcriptional circuit operating in a multicellular organism, we must disentangle the influences of positional information (where inputs are expressed) and regulatory logic (how inputs are interpreted). By separating these influences we were able to detect fine-scale differences in the functions of the orthologous CREs that wire this particular circuit. Our method can be applied to many such circuits and to regulatory sequences other than CREs.

Our method uses cellular resolution measurements of both the inputs and output of a transcriptional circuit in three species. We found that expression pattern divergence is largely explained by changes in the expression patterns of the input TFs. We used transgenic experiments to confirm that these orthologous CREs direct highly similar, but quantitatively distinct expression patterns. We used this transgenic data set to develop a sequence-based calculation of CRE regulatory function. Applying this calculation in the transgenic context, we showed that sequence changes in orthologous CREs alter sensitivity to their input TFs. Applying this calculation in the endogenous context, we attributed the observed expression divergence between *dmel* and *dyak* to a combination of changes in the expression patterns of regulating TFs and sequence changes in the CRE. In the context of the *dmel*/*dpse* comparison, we concluded that either (1) components in the regulatory circuit other than the input TF expression patterns and the CRE have diverged between *dmel* and *dpse*, or (2) TFs functionally diverge between these species.

A framework for contextualizing quantitative gene expression divergence

Our approach requires measuring expression in both endogenous and transgenic contexts. Endogenous expression patterns are the biologically relevant outputs of the entire transcriptional network, but they are difficult to compare across species since many parts of the network change simultaneously. In transgenic animals, the expression pattern of a reporter gene under the control of a particular regulatory element is easier to interpret, since the animals will only vary in the sequence of the test element. However, in isolation, these elements may not function as they do in the endogenous context. In fact, reporter constructs often do not recapitulate the native expression pattern precisely (discussed below). We combined these two types of measurements in a unified computational framework to assess sources of quantitative expression divergence between species. We used the endogenous measurements to fit a function relating the concentration of inputs to output for an individual transcriptional circuit and assessed the conservation of this circuit across species. We used the transgenic measurements to develop an appropriate calculation for one component of this circuit—the underlying CRE—and applied this calculation in the endogenous context to learn how it contributes to the observed expression pattern.

Quantitating sensitivity to sequence perturbation

A major unresolved question is whether there is a 'grammar' to the arrangement of TF binding sites in CREs: are particular binding site compositions, orders, or spacing more or less effective in the control of gene expression? The answer to this question is critical for understanding the molecular mechanism by which CREs operate and the constraints under which they evolve. Of the few CREs that have been dissected in detail (Arnosti *et al*, 1996; Swanson *et al*, 2010; Struffi *et al*, 2011), examples range from those with a stringent requirement for a particular arrangement of sites, e.g., the enhanceosome (Thanos and Maniatis, 1995), to examples where multiple sequence arrangements appear to be functional, e.g., the *even-skipped* stripe 2 enhancer (Ludwig *et al*, 2000; Hare *et al*, 2008a). Our finding that the set of orthologous *hb* posterior stripe CREs vary quantitatively in their function emphasizes that sensitivity to binding site arrangement is a continuous rather than a discrete property. This is consistent with previous work on neurogenic ectoderm CREs, which found that their response to inputs could be fine-tuned over evolution (Crocker *et al*, 2008). CREs therefore do not need to be classed as either sensitive or insensitive to sequence changes; using our computational framework, their sensitivity can be precisely quantitated in terms of their response to individual inputs.

Regulatory information may be dispersed throughout the *hb* locus

The pattern produced by the *dmel* transgenic line differs in both dynamics and shape from the endogenous *dmel hb* expression pattern (Figure 4B). This discordance might be due to the differences between the reporter construct and the endogenous locus: the constructs use a non-endogenous promoter; the CRE is ~40 bp away from the promoter in the transgenic construct and ~3000–6000 bp away in the endogenous locus; and the constructs use a reporter gene, *lacZ*, which may show different transcription and degradation rates compared with the *hb* transcript. Alternatively, the constructs may omit relevant regulatory sequence. The use of transgenic reporters is widespread (Ludwig *et al*, 2005; Crocker *et al*, 2008; Hare *et al*, 2008a), making these discrepancies notable, especially for studies where quantitative differences are important.

Several pieces of evidence suggest that transgenic constructs may be missing relevant regulatory sequence. First, the CREs from other species drive more expression in the anterior region than the orthologous *dmel* CRE in the transgenic animals (Supplementary Figure 8). This variability does not correlate with variability in anterior expression in the endogenous context (Supplementary Figure 5), implying that this additional expression is masked in the endogenous context by repressive signals located elsewhere in the *hb* locus. Second, the idea of dispersed regulatory information is consistent with the recent identification of 'shadow' enhancers, or CREs in the same locus that drive similar expression patterns, reviewed in Barolo (2012). The discovery of many shadow enhancers suggests that regulatory information is generally not limited to the classically identified CREs (Kazemian *et al*, 2010). In support of this view, experimental *in-vivo* binding measurements show that regulatory TFs often bind outside annotated CREs (Li *et al*, 2008), and it remains unclear why these binding events would be non-functional. In addition, scattered blocks of conservation have been found outside the annotated regulatory elements in both the *eve* and *bric-a-brac* loci (Hare *et al*, 2008a; Bickel *et al*, 2011).

A number of additional experiments may help elaborate the location and mechanism of integration of regulatory information in a locus like *hb*. To rule out the role of reporter construct artifacts, reporters that more closely reflect the endogenous *hb* locus with regard to promoter sequence, UTR sequences, and promoter-CRE spacing can be constructed. These additional sequences could also be isolated from the other species and compared in the transgenic context to determine if any of them contribute to expression differences. Our modeling framework can easily accommodate additional parameters that describe the influence of these components on the output. It will also be informative to look at the behavior of a reporter engineered into a construct that includes larger pieces of the *hb* locus, an experiment enabled by the availability of BAC libraries for several Drosophilids (Ejsmont *et al*, 2009; Song *et al*, 2011).

Other contributions to expression divergence

Our modeling framework allows us to separate the contributions of positional information and regulatory logic to the observed differences in *hb*'s expression pattern between species. Implicit in the calculation of the sequence weight is the assumption that other aspects of the network, namely the potencies of the regulators (***p***) and their DNA binding preferences, are conserved between species. We made this assumption based on two observations: the strong sequence conservation between orthologous TFs in these species and the similar behavior of orthologous *cis*-regulatory sequences in the same transgenic *dmel* context. However, neither of these observations tests this assumption explicitly. Though it is hard to directly measure a regulator's potency, a data set that includes all four *hb* CREs in all four transgenic species environments would allow us to infer each regulator's potency in each species. Though transgenic technology is most facile in *dmel*, it is possible to make transgenics in an increasing number of Drosophilids (Holtzman *et al*, 2010).

The high level of sequence conservation in the DNA binding domains of input TFs suggests that their DNA binding specificity is virtually identical, but our sequence weight calculation is limited by available data. We used position weight matrices (PWMs) that describe the binding preferences for *dmel* proteins to calculate the sequence weights for each CRE (Bergman *et al*, 2005). Though this calculation is technically correct for the transgenic experiments, ideally, we would use PWMs describing the binding preferences of the TFs from *dmel*, *dyak*, and *dpse* in the sequence weight calculations in the endogenous context. However, even if DNA binding specificities prove to be identical, changes outside of the DNA binding domain may also affect gene expression through other means, like changes in protein–protein interactions. These are harder to measure with current techniques, but are critical for a detailed understanding of the evolution of this network.

Another limitation of our method is the use of relative expression measurements. In fitting a model in a single species, absolute measurements are unnecessary because fit parameters include the effect of concentration differences between regulators. However, absolute concentrations of the same gene in different species may vary. This would manifest in two ways. First, differences in expression levels may contribute to variation in the parameter values of the 'best fits' for sets of orthologous regulators (see Table I). Second, when parameters fit in one species are applied to another, differences in expression level may contribute to a decrease in the 'applied fits'. As imaging technologies improve, it is likely that obtaining absolute measures of expression will become routine and will circumvent this issue.

A simple modeling framework for comparative analysis of transcriptional circuits

We began our study with a circuit level model of the *hb* posterior stripe that was agnostic to sequence information. Other sequence-agnostic models of the regulatory network have been used to study other facets of the system, e.g., the topology and the manner in which canalization is achieved (Perkins *et al*, 2006; Manu *et al*, 2009). However, due to their interconnected, network level properties, these models are not suitable for determining the sources of expression divergence in a single circuit. Our model, while less detailed than these

previous models, was constructed specifically to allow us to dissect the sources of quantitative expression differences between species. Given the complexity of transcriptional regulation, it is likely that no single modeling framework will be appropriate for every question (Wunderlich and DePace, 2011). We anticipate that the increase in quantitative, systematic data for transcriptional networks will be accompanied by an increase in models appropriate for different biological questions.

To account for the regulatory sequence contribution to gene expression divergence, we developed a simple measure of relative CRE sequence function. Other predictive models of *Drosophila* CRE function have been developed by fitting many different types of CREs simultaneously, using a thermodynamic framework (Segal *et al*, 2008; He *et al*, 2010). These studies systematically assessed the influence of cooperativity and local binding site arrangement on CRE output. However, they are not accurate enough to predict subtle quantitative differences in expression observed between closely related species, and sometimes fail to predict expression of orthologous CREs entirely. By fitting the same parameters to different types of CREs, context-dependent rules may be obscured, e.g., TFs that act as activators in one context and repressors in another appear to have average activities of zero.

Here, we take a fundamentally different approach by comparing activities of orthologous CREs from closely related species, where we can assume orthologous sequences are built using similar rules. When done systematically for many CREs, this approach may be particularly useful for discerning rules of CRE architecture. By characterizing natural sequence variants that have been filtered by evolution to be functional but differ quantitatively, we likely need to examine many fewer sequences than if we were to characterize a random collection of synthetic CREs. In support of this argument, work from Fakhouri *et al* (2010) has shown than synthetic CREs built from a limited number of components and designed to test the influence of local sequence arrangement can be useful for discovering specific rules about CRE architecture.

Our approach of comparing relative CRE sequence function can also be used to suggest new experiments. We can calculate the sequence weights of the *hb* posterior stripe CRE in other sequenced species and use them to predict expression patterns. This approach can focus time-intensive experiments on relevant subsets of CREs. We are particularly interested in CREs with pervasive sequence rearrangements and conserved output as well as those with small-scale sequence changes and divergent output.

It is notable that a linear model captures critical aspects of *hb* regulation. The importance of cooperativity and synergy in this system have been well documented (Simpson-Brose *et al*, 1994; Arnosti *et al*, 1996; Burz *et al*, 1998; He *et al*, 2010). Since non-linear effects can produce sharp, narrow stripes of gene expression, it is possible that they are less important for the graded expression patterns of the gap genes and are more important for the expression of sharply defined expression patterns, such as the pair-rule genes. The linear model also implies that the effects of the regulators on the output are additive in this setting, suggesting that the 'information display' model of CRE interpretation may be at play at this locus (Kulkarni and Arnosti, 2003). Though the linear model represents a simplification, it recapitulates known features of *hb* regulation. For example, Ashyraliyev *et al* (2009) identify the importance of *hkb* in setting the posterior border of *hb* expression. By dropping regulators from our model, both individually and in pairs, we also observe the importance of *hkb* in the accurate prediction of *hb* expression (Supplementary Figure 6).

Interpretation of coefficients

Aside from the five regulators included as inputs, there is evidence that other TFs are important for the formation of the *hb* posterior stripe, e.g., *caudal* and *Zelda* (Jaeger, 2011; Nien *et al*, 2011). We excluded both *Zelda* and *caudal* because their expression patterns have not been measured in the relevant species. *Zelda* is expressed in a uniform pattern in the embryo (Liang *et al*, 2008), so any contribution to inter-species divergence would be from changes in its level, a quantity better assessed by other experimental techniques, e.g., qPCR or quantitative western blot. In its current form, the effects of both of these activators, as well as other factors are included in the constant term in Equations (3) and (4). We calculated the sequence weight for *caudal*, which is 1.10 for *dyak* and 0.79 for *dpse* and *dper*. The constant values for *dmel*, *dyak*, and *dpse* are 0.4833, 0.5688, and 0.4293, respectively, which show a qualitative trend similar to that of the *caudal* sequence weight, providing circumstantial evidence that our interpretation of the constant term is correct.

Sources of upstream variation in the anterior-posterior patterning system

Our model does not address the sources of the positional variation of *hb*'s regulators, but our data set may be useful for addressing this question. One possibility is that variation in the morphology of the embryos, in terms of shape, nuclear number, and density has ramifications for the output of this patterning system. Our data set spans embryos with variation in nuclear number (species averages range from 5087 ± 327 to 6128 ± 348 nuclei), egg length (394 ± 31 to 452 ± 23 microns), and embryo surface area ($143\,000 \pm 12\,100$ to $198\,000 \pm 16\,000$ microns^2) (Fowlkes *et al*, 2011). A different type of model that includes morphogen behavior in this range of morphological contexts might prove useful for addressing this issue. Other possible sources of variation include translation rates, degradation rates, and post-translational modifications. These control mechanisms operate in this system (Tautz and Pfeifle, 1989; Thomsen *et al*, 2010; Kim *et al*, 2011) and could potentially be included in this framework.

Connecting regulatory sequence and function

In previous work, we measured the expression patterns of several key TFs and developed a metric to compare cellular gene expression profiles pair-wise between three species (Fowlkes *et al*, 2011). The cellular gene expression profile reflects the input/output relationship of many CREs operating in the system. Therefore, the expression distance metric we developed provides a global view of regulatory similarity

between the three species. However, without further analysis the similarities and differences are not attributable to any particular input/output function. In this study, we undertook a detailed analysis of a particular input/output function using our comparative data. Our results are consistent with the view provided by the expression distance metric, where the cells near the *hb* posterior stripe were identified as having similar cellular gene expression profiles. Comparison of cellular gene expression profiles may prove to be a relatively simple and unbiased way to pinpoint conserved and divergent regulatory functions for further study.

Determining the origins of quantitative expression differences between species will advance our understanding of transcriptional regulation in two ways. First, linking sequence changes to quantitative differences in expression patterns for many CREs may identify rules governing enhancer architecture. CREs in this system have been extensively annotated using transgenic experiments (Gallo *et al*, 2011), functional genomic data (Consortium *et al*, 2010; Kvon *et al*, 2012), and sequence conservation (Berman *et al*, 2004; Sinha *et al*, 2004; Odenwald *et al*, 2005). Application of our method to other CREs in additional species is a clear future direction. Second, understanding how transcriptional circuits evolve, both in terms of their overall output and in terms of their individual components, will provide insights into how genetic changes are either amplified or buffered to influence generation of new phenotypes. Our experimental and computational approach lays the groundwork for these goals.

Materials and methods

Identification of predicted transcription binding sites

To identify predicted TF binding sites for Figure 1B, we used Patser (http://ural.wustl.edu/software.html), with a GC content of 0.406, a *P*-value cutoff of 0.003, and PWMs derived from Bergman *et al* (2005).

Creation of transgenic flies

We used the *dmel hb* posterior stripe CRE identified in Berman *et al* (2004), element hb_Hz1.4, with an ~100 bp buffer on each side to ensure completeness (Release 5 coordinates 3R:4526471-4528036). Orthologous CREs were identified using the genome-wide alignments available in the UCSC Genome Browser (Fujita *et al*, 2011) and the coordinates are as follows: dyak: 3R:8589892-8591517 (Nov. 2005 assembly), dpse: 2:27088673-27090287 (Nov. 2005 assembly), and dper: super_6:2470507-2472121 (Oct. 2005 assembly). The four posterior stripe CREs were amplified from genomic DNA libraries from the sequenced lines (Drosophila Species Stock Center, https://stockcenter.ucsd.edu) using primers that contain species-specific sequences and synthetic cut sites for *Not*I and *Bgl*II, with the exception of the *dmel* posterior stripe CRE. The *dmel* CRE sequence contained a *Bgl*II cut site, so *Not*I was used on both ends. Each PCR product was digested with *Bgl*II and/or *Not*I and inserted into the multiple cloning site of the pBΦY vector (Hare *et al*, 2008a). The pBΦY vector contains the *dmel eve* basal promoter (2R:5866782-5866986) driving *lacZ* and also has the attB site necessary for site-specific integration using the ΦC31 system (Fish *et al*, 2007). Each plasmid was then co-injected with the ΦC31 integrase into w^{118} flies carrying the attP2 integration site (Groth *et al*, 2004) by Genetic Services, Inc. Transformant flies were then homozygosed.

In-situ hybridization

Whole mount *in-situ* hybridization was performed as described in Luengo Hendriks *et al* (2006). In brief, 0–4 h old embryos (25°C) were collected, dechorionated, fixed in a mixture of formaldehyde and heptane, and devitellinized in a mixture of heptane and methanol. Embryos were then post-fixed in formaldehyde and washed several times in a formamide-based hybridization buffer. The embryos were incubated at 56°C with two full-length cDNA probes, a DIG-labeled probe for the fiduciary marker, *fushi tarazu* (*ftz*), and a DNP-labeled probe for *lacZ*. The embryos were then successively stained using anti-DIG-HRP (anti-DIG-POD; Roche, Basil, Switzerland) and anti-DNP-HRP (Perkin-Elmer TSA-kit, Waltham, MA, USA) antibodies, using reactions with coumarin- and Cy3-tyramide (Perkin-Elmer). To stain the nuclei, embryos were treated with RNaseA and then stained with Sytox Green (Invitrogen, Carlsbad, CA, USA). The embryos were mounted in DePex (Electron Microscopy Sciences, Hatfield, PA, USA), using a bridge of #1 coverslips to preserve embryo morphology.

Image acquisition, image processing, and atlas creation

Stained and mounted embryos were imaged and processed using the methods described in Luengo Hendriks *et al* (2006) and Fowlkes *et al* (2008). Briefly, the three-dimensional image stacks of each embryo were acquired using 2-photon laser scanning microscopy on a Zeiss LSM 710 with a plan-apochromat 20×0.8 NA objective. Using the software described in Luengo Hendriks *et al* (2006), each image file was converted into a PointCloud, a text file that includes the location and levels of gene expression for each nucleus in the embryo.

Using the expression pattern of the fiduciary marker *ftz*, embryos were registered to a representative embryo (template) with the methods described in Fowlkes *et al* (2008). The registered embryos were then combined with the data from Fowlkes *et al* (2008) to create a gene expression atlas, a text file that contains the average expression values of *hb*'s five regulators and the *lacZ* output from each of the four transgenic lines in each cell of the embryo. The gene expression atlas includes data from 64 embryos from the *dmel* line, 57 embryos from the *dyak* line, 52 embryos from the *dpse* line, and 51 embryos from the *dper* line. Each time point average included the data from at least 4 embryos, with an average of 10 embryos per time point. These blastoderm-stage embryos were sorted into time points by visualizing them using phase contrast optics and observing the degree of membrane invagination. The six, ~10 min time points correspond to 0–3%, 4–8%, 9–25%, 26–50%, 51–75%, and 76–100% membrane invagination and were judged by using the side of the embryo where membrane invagination is the furthest progressed.

Characterization of stripe boundary positions and size

The analysis of *hb* posterior stripe boundary positions and the number of cells in the stripe was done in MATLAB using the PointCloud toolbox (http://bdtnp.lbl.gov/Fly-Net/bioimaging.jsp?w = analysis). Using the stripe finding functions included in the toolbox, we located the stripes in each individual PointCloud used to construct the gene expression atlases, and we then recorded the boundary positions and number of cells located in each embryo's stripe.

Modeling of *hb* posterior stripe

To carry out the modeling of the posterior stripe, MATLAB was used to implement standard multiple linear regression techniques using the glmfit command. The matrix of independent variables had a row for each cell at each time point and five columns corresponding to the relative expression levels of each of the five regulators used in the study. The dependent variable vector had an equal number of rows and one column corresponding to the level of *lacZ* or *hb* in each cell at each time point.

To calculate the ROC AUC, we calculated the ROC curve by first thresholding the experimental data. The threshold was calculated as the mode of the target expression data plus one standard deviation:

$$\text{threshold}(s) = \text{mode}(\text{lacZ}(i, s, t))_{i,t} + \text{std}(lacZ(i, s, t))_{i,t} \quad (7)$$

Then, one species at a time, we varied the threshold applied to the predictions of the linear model, considering all points below the threshold as an 'off' prediction, and all points above the threshold as an 'on' prediction. For each threshold, we calculated the true positive rate, i.e., the fraction of experimentally verified 'on' cells that are predicted correctly, and the false positive rate, i.e., the fraction of the experimentally 'off' cells that are predicted incorrectly. We plot the true positive rate as a function of the false positive rate and calculate the area underneath the curve using the trapezoidal rule. To calculate the statistical significance of an individual ROC AUC, we use the non-parametric Mann–Whitney *U*-test. To compare the values of two ROC AUCs, we use a test based on the Mann–Whitney *U*-test, as implemented in the StAR software (Vergara *et al*, 2008).

To do the 10-fold cross-validation, either the *dmel* endogenous or the transgenic data set was used. The data set was split into 10 roughly equal fractions. In turn, each fraction was left out of the set used to train the multiple linear regression, and then used to evaluate the resulting model.

Calculation of sequence weights

To calculate the sequence weight of a given sequence for a given TF $\boldsymbol{c}(s)$, we use the following formula

$$\boldsymbol{c}(s) = \frac{\sum_{i=1}^{l-w+1} \prod_{j=1}^{w} \frac{p_i(b(i))}{q(b(i))}}{c(dmel)} \quad (8)$$

Here, l is the length of the sequence being considered, w is the width of the PWM of the TF, $b(i)$ is the base at position i of the sequence, $p_j(b)$ is the frequency of seeing base b at position j of the PWM, and $q(b)$ is the background frequency of base b. When multiplied by a concentration, this value is roughly proportional to the total number of TF molecules bound to a sequence, assuming the sites are not saturated (Supplementary information). To look for saturated binding sites, i.e., very strong sites that will be occupied with a high probability even at low concentrations of TF, we searched for binding sites that accounted for 50% or more of the total value of the sequence weight and found a single *hkb* site in the *dyak* posterior stripe CRE that fit this criteria. To avoid the presumably unrealistic impact of this single binding site, we thresholded its value to its 99th percentile value.

Here, we again use a background GC content = 0.406 and the PWMs from Bergman *et al* (2005). The sequence weights we use in our model $\boldsymbol{c}(s)$ are vectors of length 5, with each entry consisting of the sequence weight for one of the five regulators. We compared the performance of these PWMs with those derived from bacterial one-hybrid (Noyes *et al*, 2008) and SELEX (Li *et al*, 2011) experiments. The qualitative performance of the model is independent of the PWM set used and is discussed in more detail in Supplementary Figure 10. We chose to use the PWMs from Bergman *et al* (2005) as they gave the highest performance on the transgenic lines. To calculate the sequence weights for the posterior stripe CRE, we used the sequences in our transgenic constructs.

Supplementary information

Supplementary information is available at the *Molecular Systems Biology* website (www.nature.com/msb).

Acknowledgements

We thank Charless Fowlkes for advice on building gene expression atlases and Cris Luengo Hendriks for help using the PointCloud toolbox and advice on analyzing the PointCloud data shown in Supplementary Figure 1. Miriah Meyer wrote the InSite software used to create Figure 1B, which is available at www.cs.utah.edu/~miriah/insite/. The image processing in this paper was run on the Orchestra cluster supported by the Harvard Medical School Research Information Technology Group. We thank Robert Bradley, Amelia Green, Jeremy Gunawardena, Rishi Jajoo, Nickolay Khazanov, Leonid Mirny and the members of the DePace lab, particularly Ben Vincent and Max Staller, for their helpful discussions and suggestions on the manuscript. We also thank the anonymous reviewers for their many helpful suggestions for improving the manuscript.

Author contributions: ZW and AHD conceived and designed the experiments. ZW, TLM, and SPW created the transgenic flies. ZW and KBE conducted the *in-situ* hybridizations. ZW and MDB imaged the embryos. ZW analyzed the data. ZW and AHD wrote the manuscript.

References

Ardehali MB, Lis JT (2009) Tracking rates of transcription and splicing *in vivo*. *Nat Struct Mol Biol* **16:** 1123–1124

Arnosti DN, Barolo S, Levine M, Small S (1996) The eve stripe 2 enhancer employs multiple modes of transcriptional synergy. *Development* **122:** 205–214

Ashyraliyev M, Siggens K, Janssens H, Blom J, Akam M, Jaeger J (2009) Gene circuit analysis of the terminal gap gene huckebein. *PLoS Comput Biol* **5:** e1000548

Barolo S (2012) Shadow enhancers: frequently asked questions about distributed cis-regulatory information and enhancer redundancy. *Bioessays* **34:** 135–141

Ben-Tabou de-Leon S, Davidson EH (2007) Gene regulation: gene control network in development. *Annu Rev Biophys Biomol Struct* **36:** 191

Bergman C, Carlson JW, Celniker SE (2005) Drosophila DNase I footprint database: a systematic genome annotation of transcription factor binding sites in the fruitfly, Drosophila melanogaster. *Bioinformatics* **21:** 1747–1749

Berman BP, Pfeiffer BD, Laverty TR, Salzberg SL, Rubin GM, Eisen MB, Celniker SE (2004) Computational identification of developmental enhancers: conservation and function of transcription factor binding-site clusters in Drosophila melanogaster and Drosophila pseudoobscura. *Genome Biol* **5:** R61

Bickel RD, Kopp A, Nuzhdin SV (2011) Composite effects of polymorphisms near multiple regulatory elements create a major-effect QTL. *PLoS Genet* **7:** e1001275

Brem RB, Yvert G, Clinton R, Kruglyak L (2002) Genetic dissection of transcriptional regulation in budding yeast. *Science* **296:** 752–755

Burz DS, Rivera-Pomar R, Jackle H, Hanes SD (1998) Cooperative DNA-binding by Bicoid provides a mechanism for threshold-dependent gene activation in the Drosophila embryo. *EMBO J* **17:** 5998–6009

Casanova J (1990) Pattern formation under the control of the terminal system in the Drosophila embryo. *Development* **110:** 621–628

Chan YF, Marks ME, Jones FC, Villarreal G, Shapiro MD, Brady SD, Southwick AM, Absher DM, Grimwood J, Schmutz J, Myers RM, Petrov D, Jónsson B, Schluter D, Bell MA, Kingsley DM (2010) Adaptive evolution of pelvic reduction in sticklebacks by recurrent deletion of a Pitx1 enhancer. *Science* **327:** 302–305

Cheung VG, Spielman RS (2009) Genetics of human gene expression: mapping DNA variants that influence gene expression. *Nat Rev Genet* **10:** 595–604

modENCODE Consortium, Roy S, Ernst J, Kharchenko PV, Kheradpour P, Negre N, Eaton ML, Landolin JM, Bristow CA, Ma L, Lin MF, Washietl S, Arshinoff BI, Ay F, Meyer PE, Robine N, Washington NL, Di Stefano L, Berezikov E, Brown CD, Candeias R *et al* (2010) Identification of functional elements and regulatory circuits by Drosophila modENCODE. *Science* **330:** 1787–1797

Crocker J, Erives A (2008) A closer look at the eve stripe 2 enhancers of Drosophila and Themira. *PLoS Genet* **4:** e1000276

Crocker J, Tamori Y, Erives A (2008) Evolution acts on enhancer organization to fine-tune gradient threshold readouts. *PLoS Biol* **6:** e263

Ejsmont RK, Sarov M, Winkler S, Lipinski KA, Tomancak P (2009) A toolkit for high-throughput, cross-species gene engineering in Drosophila. *Nat Methods* **6:** 435–437

Fakhouri WD, Ay A, Sayal R, Dresch J, Dayringer E, Arnosti DN (2010) Deciphering a transcriptional regulatory code: modeling short-range repression in the Drosophila embryo. *Mol Syst Biol* **6:** 341

Fish MP, Groth AC, Calos MP, Nusse R (2007) Creating transgenic Drosophila by microinjecting the site-specific phiC31 integrase mRNA and a transgene-containing donor plasmid. *Nat Protoc* **2:** 2325–2331

Fowlkes CC, Eckenrode KB, Bragdon MD, Meyer M, Wunderlich Z, Simirenko L, Luengo Hendriks CL, Keranen SV, Henriquez C, Knowles DW, Biggin MD, Eisen MB, Depace AH (2011) A conserved developmental patterning network produces quantitatively different output in multiple species of Drosophila. *PLoS Genet* **7:** e1002346

Fowlkes CC, Hendriks CL, Keranen SV, Weber GH, Rubel O, Huang MY, Chatoor S, DePace AH, Simirenko L, Henriquez C, Beaton A, Weiszmann R, Celniker S, Hamann B, Knowles DW, Biggin MD, Eisen MB, Malik J (2008) A quantitative spatiotemporal atlas of gene expression in the Drosophila blastoderm. *Cell* **133:** 364–374

Frankel N, Erezyilmaz DF, McGregor AP, Wang S, Payre F, Stern DL (2011) Morphological evolution caused by many subtle-effect substitutions in regulatory DNA. *Nature* **474:** 598–603

Fujita PA, Rhead B, Zweig AS, Hinrichs AS, Karolchik D, Cline MS, Goldman M, Barber GP, Clawson H, Coelho A, Diekhans M, Dreszer TR, Giardine BM, Harte RA, Hillman-Jackson J, Hsu F, Kirkup V, Kuhn RM, Learned K, Li CH *et al* (2011) The UCSC Genome Browser database: update 2011. *Nucleic Acids Res* **39:** D876–D882

Gallo SM, Gerrard DT, Miner D, Simich M, Des Soye B, Bergman CM, Halfon MS (2011) REDfly v3.0: toward a comprehensive database of transcriptional regulatory elements in Drosophila. *Nucleic Acids Res* **39:** D118–D123

Goltsev Y, Fuse N, Frasch M, Zinzen RP, Lanzaro G, Levine M (2007) Evolution of the dorsal-ventral patterning network in the mosquito, Anopheles gambiae. *Development* **134:** 2415–2424

Gompel N, Prud'homme B, Wittkopp PJ, Kassner VA, Carroll SB (2005) Chance caught on the wing: cis-regulatory evolution and the origin of pigment patterns in Drosophila. *Nature* **433:** 481–487

Groth AC, Fish M, Nusse R, Calos MP (2004) Construction of transgenic Drosophila by using the site-specific integrase from phage phiC31. *Genetics* **166:** 1775–1782

Hare EE, Peterson BK, Eisen MB (2008b) A careful look at binding site reorganization in the even-skipped enhancers of Drosophila and sepsids. *PLoS Genet* **4:** e1000268

Hare EE, Peterson BK, Iyer VN, Meier R, Eisen MB (2008a) Sepsid even-skipped enhancers are functionally conserved in Drosophila despite lack of sequence conservation. *PLoS Genet* **4:** e1000106

He X, Samee MA, Blatti C, Sinha S (2010) Thermodynamics-based models of transcriptional regulation by enhancers: the roles of synergistic activation, cooperative binding and short-range repression. *PLoS Comput Biol* **6:** e1000935

Holtzman S, Miller D, Eisman R, Kuwayama H, Niimi T, Kaufman T (2010) Transgenic tools for members of the genus Drosophila with sequenced genomes. *Fly (Austin)* **4:** 349–362

Hutter S, Saminadin-Peter S, Stephan W, Parsch J (2008) Gene expression variation in African and European populations of Drosophila melanogaster. *Genome Biol* **9:** R12

Jaeger J (2011) The gap gene network. *Cell Mol Life Sci* **68:** 243–274

Jäckle H, Tautz D, Schuh R, Seifert E (1986) Cross-regulatory interactions among the gap genes of Drosophila. *Nature* **324:** 668–670

Kazemian M, Blatti C, Richards A, McCutchan M, Wakabayashi-Ito N, Hammonds AS, Celniker SE, Kumar S, Wolfe SA, Brodsky MH, Sinha S (2010) Quantitative analysis of the Drosophila segmentation regulatory network using pattern generating potentials. *PLoS Biol* **8:** e1000456

Kim J, He X, Sinha S (2009) Evolution of regulatory sequences in 12 Drosophila species. *PLoS Genet* **5:** e1000330

Kim Y, Andreu MJ, Lim B, Chung K, Terayama M, Jimenez G, Berg CA, Lu H, Shvartsman SY (2011) Gene regulation by MAPK substrate competition. *Dev Cell* **20:** 880–887

Kosman D, Small S (1997) Concentration-dependent patterning by an ectopic expression domain of the Drosophila gap gene knirps. *Development* **124:** 1343–1354

Kulkarni MM, Arnosti DN (2003) Information display by transcriptional enhancers. *Development* **130:** 6569–6575

Kvon EZ, Stampfel G, Yanez-Cuna JO, Dickson BJ, Stark A (2012) HOT regions function as patterned developmental enhancers and have a distinct cis-regulatory signature. *Genes Dev* **26:** 908–913

Lehmann R, Nüsslein-Volhard C (1987) Hunchback, a gene required for segmentation of an anterior and posterior region of the Drosophila embryo. *Dev Biol* **119:** 402–417

Li H, Johnson AD (2010) Evolution of transcription networks—lessons from yeasts. *Curr Biol* **20:** R746–R753

Li XY, MacArthur S, Bourgon R, Nix DA, Pollard DA, Iyer VN, Hechmer A, Simirenko L, Stapleton M, Luengo Hendriks CL, Chu HC, Ogawa N, Inwood W, Sementchenko V, Beaton A, Weiszmann R, Celniker SE, Knowles DW, Gingeras T, Speed TP *et al* (2008) Transcription factors bind thousands of active and inactive regions in the Drosophila blastoderm. *PLoS Biol* **6:** e27

Li XY, Thomas S, Sabo PJ, Eisen MB, Stamatoyannopoulos JA, Biggin MD (2011) The role of chromatin accessibility in directing the widespread, overlapping patterns of Drosophila transcription factor binding. *Genome Biol* **12:** R34

Liang HL, Nien CY, Liu HY, Metzstein MM, Kirov N, Rushlow C (2008) The zinc-finger protein Zelda is a key activator of the early zygotic genome in Drosophila. *Nature* **456:** 400–403

Lott SE, Kreitman M, Palsson A, Alekseeva E, Ludwig MZ (2007) Canalization of segmentation and its evolution in Drosophila. *Proc Natl Acad Sci* **104:** 10926–10931

Ludwig MZ, Bergman C, Patel NH, Kreitman M (2000) Evidence for stabilizing selection in a eukaryotic enhancer element. *Nature* **403:** 564–567

Ludwig MZ, Palsson A, Alekseeva E, Bergman C, Nathan J, Kreitman M (2005) Functional evolution of a cis-regulatory module. *PLoS Biol* **3:** e93

Luengo Hendriks CL, Keränen SV, Fowlkes CC, Simirenko L, Weber GH, DePace AH, Henriquez C, Kaszuba DW, Hamann B, Eisen MB, Malik J, Sudar D, Biggin MD, Knowles DW (2006) Three-dimensional morphology and gene expression in the Drosophila blastoderm at cellular resolution I: data acquisition pipeline. *Genome Biol* **7:** R123

Lukowitz W, Schröder C, Glaser G, Hülskamp M, Tautz D (1994) Regulatory and coding regions of the segmentation gene hunchback are functionally conserved between Drosophila virilis and Drosophila melanogaster. *Mech Dev* **45:** 105–115

Lynch J, Desplan C (2003) Evolution of development: beyond bicoid. *Curr Biol* **13:** R557–R559

Manu, Surkova S, Spirov AV, Gursky VV, Janssens H, Kim AR, Radulescu O, Vanario-Alonso CE, Sharp DH, Samsonova M, Reinitz J (2009) Canalization of gene expression in the Drosophila blastoderm by gap gene cross regulation. *PLoS Biol* **7:** e1000049

Margolis JS, Borowsky ML, Steingrimsson E, Shim CW, Lengyel JA, Posakony JW (1995) Posterior stripe expression of hunchback is driven from two promoters by a common enhancer element. *Development* **121:** 3067–3077

Maston GA, Evans SK, Green MR (2006) Transcriptional regulatory elements in the human genome. *Annu Rev Genomics Hum Genet* **7:** 29–59

McGregor AP, Orgogozo V, Delon I, Zanet J, Srinivasan DG, Payre F, Stern DL (2007) Morphological evolution through multiple cis-regulatory mutations at a single gene. *Nature* **448:** 587–590

Moses AM, Pollard DA, Nix DA, Iyer VN, Li XY, Biggin MD, Eisen MB (2006) Large-scale turnover of functional transcription factor binding sites in Drosophila. *PLoS Comput Biol* **2:** e130

Muller L, Grath S, von Heckel K, Parsch J (2012) Inter- and intraspecific variation in Drosophila genes with sex-biased expression. *Int J Evol Biol* **2012:** 963976

Nien CY, Liang HL, Butcher S, Sun Y, Fu S, Gocha T, Kirov N, Manak JR, Rushlow C (2011) Temporal coordination of gene networks by Zelda in the early Drosophila embryo. *PLoS Genet* **7:** e1002339

Noyes MB, Meng X, Wakabayashi A, Sinha S, Brodsky MH, Wolfe SA (2008) A systematic characterization of factors that regulate Drosophila segmentation via a bacterial one-hybrid system. *Nucleic Acids Res* **36:** 2547–2560

Nuzhdin SV, Tufts DM, Hahn MW (2008) Abundant genetic variation in transcript level during early Drosophila development. *Evol Dev* **10:** 683–689

Odenwald WF, Rasband W, Kuzin A, Brody T (2005) EVOPRINTER, a multigenomic comparative tool for rapid identification of functionally important DNA. *Proc Natl Acad Sci USA* **102:** 14700–14705

Perkins TJ, Jaeger J, Reinitz J, Glass L (2006) Reverse engineering the gap gene network of Drosophila melanogaster. *PLoS Comput Biol* **2:** e51

Richards S, Liu Y, Bettencourt BR, Hradecky P, Letovsky S, Nielsen R, Thornton K, Hubisz MJ, Chen R, Meisel RP, Couronne O, Hua S, Smith MA, Zhang P, Liu J, Bussemaker HJ, van Batenburg MF, Howells SL, Scherer SE, Sodergren E *et al* (2005) Comparative genome sequencing of Drosophila pseudoobscura: chromosomal, gene, and cis-element evolution. *Genome Res* **15:** 1–18

Rockman MV, Skrovanek SS, Kruglyak L (2010) Selection at linked sites shapes heritable phenotypic variation in C. elegans. *Science* **330:** 372–376

Schröder C, Tautz D, Seifert E, Jäckle H (1988) Differential regulation of the two transcripts from the Drosophila gap segmentation gene hunchback. *EMBO J* **7:** 2881

Segal E, Raveh-Sadka T, Schroeder M, Unnerstall U, Gaul U (2008) Predicting expression patterns from regulatory sequence in Drosophila segmentation. *Nature* **451:** 535–540

Simpson-Brose M, Treisman J, Desplan C (1994) Synergy between the hunchback and bicoid morphogens is required for anterior patterning in Drosophila. *Cell* **78:** 855–865

Sinha S, Schroeder MD, Unnerstall U, Gaul U, Siggia ED (2004) Cross-species comparison significantly improves genome-wide prediction of cis-regulatory modules in Drosophila. *BMC Bioinformatics* **5:** 129

Song X, Goicoechea JL, Ammiraju JS, Luo M, He R, Lin J, Lee SJ, Sisneros N, Watts T, Kudrna DA, Golser W, Ashley E, Collura K, Braidotti M, Yu Y, Matzkin LM, McAllister BF, Markow TA, Wing RA (2011) The 19 genomes of Drosophila: a BAC library resource for genus-wide and genome-scale comparative evolutionary research. *Genetics* **187:** 1023–1030

Struffi P, Corado M, Kaplan L, Yu D, Rushlow C, Small S (2011) Combinatorial activation and concentration-dependent repression of the Drosophila even skipped stripe 3 + 7 enhancer. *Development* **138:** 4291–4299

Struhl G, Johnston P, Lawrence PA (1992) Control of Drosophila body pattern by the hunchback morphogen gradient. *Cell* **69:** 237–249

Swanson CI, Evans NC, Barolo S (2010) Structural rules and complex regulatory circuitry constrain expression of a Notch- and EGFR-regulated eye enhancer. *Dev Cell* **18:** 359–370

Swanson CI, Schwimmer DB, Barolo S (2011) Rapid evolutionary rewiring of a structurally constrained eye enhancer. *Curr Biol* **21:** 1186–1196

Swets JA (1988) Measuring the accuracy of diagnostic systems. *Science* **240:** 1285–1293

Tautz D, Lehmann R, Schnürch H, Schuh R, Seifert E, Jones AK, Jackle H (1987) Finger protein of novel structure encoded by hunchback, a second member of the gap class of Drosophila segmentation genes. *Nature* **327:** 383–389

Tautz D, Pfeifle C (1989) A non-radioactive in situ hybridization method for the localization of specific RNAs in Drosophila embryos reveals translational control of the segmentation gene hunchback. *Chromosoma* **98:** 81–85

Thanos D, Maniatis T (1995) Virus induction of human IFN beta gene expression requires the assembly of an enhanceosome. *Cell* **83:** 1091–1100

Thomsen S, Anders S, Janga SC, Huber W, Alonso CR (2010) Genome-wide analysis of mRNA decay patterns during early Drosophila development. *Genome Biol* **11:** R93

Vergara IA, Norambuena T, Ferrada E, Slater AW, Melo F (2008) StAR: a simple tool for the statistical comparison of ROC curves. *BMC Bioinformatics* **9:** 265

Wittkopp PJ, Haerum B, Clark AG (2008) Regulatory changes underlying expression differences within and between Drosophila species. *Nat Genet* **40:** 346–350

Wittkopp PJ, Stewart EE, Arnold LL, Neidert AH, Haerum BK, Thompson EM, Akhras S, Smith-Winberry G, Shefner L (2009) Intraspecific polymorphism to interspecific divergence: genetics of pigmentation in Drosophila. *Science* **326:** 540–544

Wittkopp PJ, Williams BL, Selegue JE, Carroll SB (2003) Drosophila pigmentation evolution: divergent genotypes underlying convergent phenotypes. *Proc Natl Acad Sci USA* **100:** 1808–1813

Wratten NS, McGregor AP, Shaw PJ, Dover GA (2006) Evolutionary and functional analysis of the tailless enhancer in Musca domestica and Drosophila melanogaster. *Evol Dev* **8:** 6–15

Wunderlich Z, DePace AH (2011) Modeling transcriptional networks in Drosophila development at multiple scales. *Curr Opin Genet Dev* **21:** 711–718

Zinzen RP, Cande J, Ronshaugen M, Papatsenko D, Levine M (2006) Evolution of the ventral midline in insect embryos. *Dev Cell* **11:** 895–902